




Bandwidth and conversion-efficiency analysis of Kerr soliton combs in dual-pumped resonators with anomalous dispersion

E. Gasmı ¹, H. Peng ², C. Koos,² and W. Reichel ^{1,*}

¹*Institute for Analysis (IANA), Karlsruhe Institute of Technology, 76131 Karlsruhe, Germany*

²*Institute of Photonics and Quantum Electronics (IPQ), Karlsruhe Institute of Technology, 76131 Karlsruhe, Germany*



(Received 28 October 2022; revised 19 June 2023; accepted 21 June 2023; published 4 August 2023)

Kerr frequency combs generated in high- Q microresonators offer an immense potential in many applications, and predicting and quantifying their behavior, performance, and stability is key to systematic device design. Based on an extension of the Lugiato-Lefever equation we investigate in this paper the perspectives of changing the pump scheme from the well-understood monochromatic pump to a dual-tone configuration simultaneously pumping two modes. For the case of anomalous dispersion we give a detailed study of the optimal choices of detuning offsets and division of total pump power between the two modes in order to optimize single-soliton comb states with respect to performance metrics like power conversion efficiency and bandwidth. Our approach allows us also to quantify the performance metrics of the optimal single-soliton comb states and determine their trends over a wide range of technically relevant parameters.

DOI: [10.1103/PhysRevA.108.023505](https://doi.org/10.1103/PhysRevA.108.023505)

I. INTRODUCTION AND MAIN RESULTS

Optical frequency combs have revolutionized many applications, comprising optical frequency metrology [1], spectroscopy [2,3], optical frequency synthesizer [4,5], optical atomic clocks [6], ultrafast optical ranging [7], and high-capacity optical communications using massively parallel wavelength-division multiplexing (WDM) [8]. The recent and rapid development of chip-scale Kerr soliton comb generators offers the prospects of realizing highly integrated devices which offer compactness, portability, and robustness, while being amenable to mass production and featuring low power consumption [9]. Whereas Kerr soliton combs have conventionally been generated by using a monochromatic pump, dual-tone pumping configurations permit one to achieve thresholdless comb generation in both normal and anomalous dispersion regimes [10,11], while stabilizing the comb-tone spacing to a well-defined frequency [12,13]. Besides, introducing the second pumped mode can maintain the intracavity power constant and eliminate the sudden change of the cavity temperature after the transition into soliton regime. Such a scheme overcomes the cavity resonance drift due to the thermo-optic effect, leading to significantly increased soliton access range [14]. The dual mode pumping scheme can be implemented either by using a phase- or intensity-modulated continuous-wave laser or two lasers with different wavelengths. Prior works theoretically investigated the dynamical properties of dissipative cavity soliton generation in a dual-mode-pumped Kerr microresonator by using the Lugiato-Lefever equation (LLE) with the addition of a secondary pump term [15]. However, a comprehensive study of the optimal pumping conditions for attaining the broadest

comb bandwidth and the highest power conversion efficiency in the anomalous dispersion regime is still lacking.

In this paper we study a variant of the LLE based on a modification for dual-tone pumping [16], and we use this equation for a more detailed study of the benefits of dual-tone pumping. Focusing on resonators with anomalous dispersion, we find that dual-tone pumping allows one to significantly improve key performance metrics of Kerr frequency combs such as bandwidth and power conversion efficiency. Mathematically, Kerr comb dynamics with a single pumped mode have been described by the LLE, a damped, driven, and detuned nonlinear Schrödinger equation [17–19]. Our modification of the LLE arises due to a forcing term which describes the pumping of two resonator modes instead of only a single one.

Using this equation as a base, we exploit numerical path continuation methods for a more detailed analysis of comb properties, the results of which can be summarized as follows.

(1) We show that with respect to comb spectral coverage, pumping two modes is advantageous to pumping only one mode.

(2) We present heuristic insights for finding the optimal detuning parameters that provide the most localized single-soliton states.

(3) We determined the optimal power distribution between the two pumped modes, which corresponds to a symmetric distribution where 50% of the power is pumped into each mode.¹ This power distribution simultaneously optimizes all performance metrics (comb bandwidth, full width at half maximum in time domain, and power conversion efficiency) in

¹For purposes of simplifying the analysis this was exactly the case discussed by the authors in [10]. Our findings validate their assumption of the pumps having equal amplitude and phase detuning.

*wolfgang.reichel@kit.edu

case equal detuning offsets between pump tones and nearest resonant modes are used.

(4) Under optimal power distribution we determined trends of the performance metrics with respect to varying dispersion and normalized total pump power.

This paper is organized as follows. In Sec. II we introduce the Lugiato-Lefever model for a dual-pumped ring resonator with second-order dispersion. In Sec. III we present the main ideas for finding localized solitons in the case of pumping two adjacent modes in the anomalous-dispersion case. Section IV is dedicated to the determination of the optimal power distribution between the two pumped modes. Here we use the comb bandwidth, the power conversion efficiency, and the full width at half maximum as performance metrics. In Sec. V we provide trends for varying dispersion or forcing of these performance metrics under the provision of optimal equal power distribution between the two pumped modes. In Sec. VI we describe the optimal solitons achieved by pumping two arbitrarily distanced modes while maintaining second-order dispersion. Appendix A is dedicated to the derivation of the Lugiato-Lefever model for a dual-pumped ring resonator. In Appendix B we explain the necessary modifications to treat the case of pumping two arbitrarily distanced modes.

II. LUGIATO-LEFEVER MODEL FOR A DUAL-PUMPED RING RESONATOR

Kerr comb dynamics are described by the LLE, a damped, driven, and detuned nonlinear Schrödinger equation [17–19]. As in [16] we use a variant of the LLE modified for two-mode pumping, for which we provide a derivation of Eq. (1) starting from a system of nonlinear coupled-mode equations in physical quantities in Appendix A. Using dimensionless, normalized quantities, this equation takes the form

$$i \frac{\partial a}{\partial \tau} = -da'' - (i - \zeta_0)a - |a|^2 a + if_0 + if_1 e^{i(k_1 x - \nu_1 \tau)}. \quad (1)$$

Here, $a(\tau, x)$ is 2π periodic in x and represents the optical intracavity field as a function of normalized time $\tau = \kappa t/2$ and angular position $x \in [0, 2\pi]$ within the ring resonator. The constant $\kappa > 0$ describes the cavity decay rate and $d = 2d_2/\kappa > 0$ quantifies the anomalous dispersion in the system ($2d_2$ corresponds to the difference between two neighboring FSRs at the center frequency ω_0). Since the numbering $k \in \mathbb{Z}$ of the resonant modes in the cavity is relative to the first pumped mode $k_0 = 0$ we denote with $k_1 \in \mathbb{N}$ the second pumped mode (there is no loss of generality to take k_1 as a positive integer since k_1 and $-k_1$ are symmetric modes). Since there are now two pumped modes there will also be two normalized detuning parameters denoted by $\zeta_0 = 2(\omega_0 - \omega_{p_0})/\kappa$ and $\zeta_1 = 2(\omega_{k_1} - \omega_{p_1})/\kappa$. They describe the offsets of the input pump frequencies ω_{p_0} and ω_{p_1} to the closest resonance frequency ω_0 and ω_{k_1} of the microresonator, respectively. Finally f_0, f_1 represent the normalized power of the input pumps. If we set $\Delta\zeta = \zeta_0 - \zeta_1$ and $\nu_1 = \Delta\zeta + dk_1^2$, then (after several transformations; cf. Appendix A) Eq. (1) emerges with the specific form of the second pump $f_1 e^{i(k_1 x - \nu_1 \tau)}$.

In the case $f_1 = 0$, Eq. (1) amounts to the case of pumping only one mode. This case has been thoroughly studied, e.g., in [18–27]. In this paper we are interested in the case

$f_1 \neq 0$. The particular form of the pump term $if_0 + if_1 e^{i(k_1 x - \nu_1 \tau)}$ suggests performing a change of variables into a moving coordinate $s = x - \omega\tau$ with $\omega = \nu_1/k_1$ and studying solutions of (1) of the form $a(\tau, x) = u(x - \omega\tau)$. These traveling-wave solutions propagate with speed ω in the resonator, and their profile u solves the stationary ordinary differential equation

$$-d u'' + i\omega u' - (i - \zeta_0)u - |u|^2 u + if_0 + if_1 e^{ik_1 s} = 0, \quad (2)$$

where u is again 2π periodic in s . In Fourier modes a and u are represented as $a(\tau, x) = \sum_{k \in \mathbb{Z}} \hat{a}_k(\tau) e^{ikx}$ and $u(s) = \sum_{k \in \mathbb{Z}} \hat{u}_k e^{iks}$. The intracavity power P of the field a at time τ is given by

$$P = \sum_{k \in \mathbb{Z}} |\hat{a}_k(\tau)|^2 = \frac{1}{2\pi} \int_0^{2\pi} |a(\tau, x)|^2 dx.$$

Since the Fourier modes of a and u are related by $\hat{a}_k(\tau) = \hat{u}_k e^{-ik\omega\tau}$ one finds $P = \sum_{k \in \mathbb{Z}} |\hat{u}_k|^2 = \frac{1}{2\pi} \int_0^{2\pi} |u(s)|^2 ds$. In particular, P is independent² of the time, and since $\int_0^{2\pi} |u|^2 ds = \text{Re} \int_0^{2\pi} (f_0 + f_1 e^{ik_1 s}) \bar{u} ds$ we see that $P \leq f^2 := f_0^2 + f_1^2$, i.e., the intracavity power cannot exceed the normalized total input power. Details are given at the end of Appendix A. Here, the notation \bar{z} denotes the complex conjugate of the complex number $z \in \mathbb{C}$.

III. FINDING LOCALIZED SOLITONS IN THE CASE OF PUMPING TWO ADJACENT MODES

In the following section, we explain the main idea for finding strongly localized solutions of (2), where two adjacent modes are pumped, i.e., the pumped modes are $k_0 = 0$ and $k_1 = 1$. The parameters $d > 0$, $k_1 = 1$, f_0 , and f_1 are fixed, and our goal is to find optimally localized solutions by varying the parameters ζ_0 and ω since they can be influenced by the choice of the pump frequencies ω_{p_0} and ω_{p_1} through the relations

$$\zeta_0 = \frac{2}{\kappa}(\omega_0 - \omega_{p_0}), \quad \omega = \frac{2}{\kappa}[\omega_0 - \omega_{p_0} - (\omega_1 - \omega_{p_1}) + d_2].$$

Optimality is understood as minimality with respect to the full width at half maximum (FWHM) of the field distribution $|u|^2$ in the time domain. We have used the MATLAB package `pde2path` (cf. [28,29]), which has been designed to numerically treat continuation and bifurcation in boundary value problems for systems of partial differential equation (PDE).³

In short, our algorithm is as follows. We initialize by determining a single-peak solution for the correct value of the parameter f_1 (ignoring the values of the parameters ζ_0 and ω). Then we alternately run an optimization algorithm with

²In fact, the power $|\hat{u}_k|^2 = |\hat{a}_k(\tau)|^2$ in each mode is independent of time.

³Continuation and bifurcation solvers for boundary value problems (on which `pde2path` is based) allow one to globally study the variety of different stationary comb states by exploiting the full range of technically available parameters. In contrast, time-integration solvers mostly only allow one to access specific comb states which strongly depend on the chosen device parameters and initial conditions.

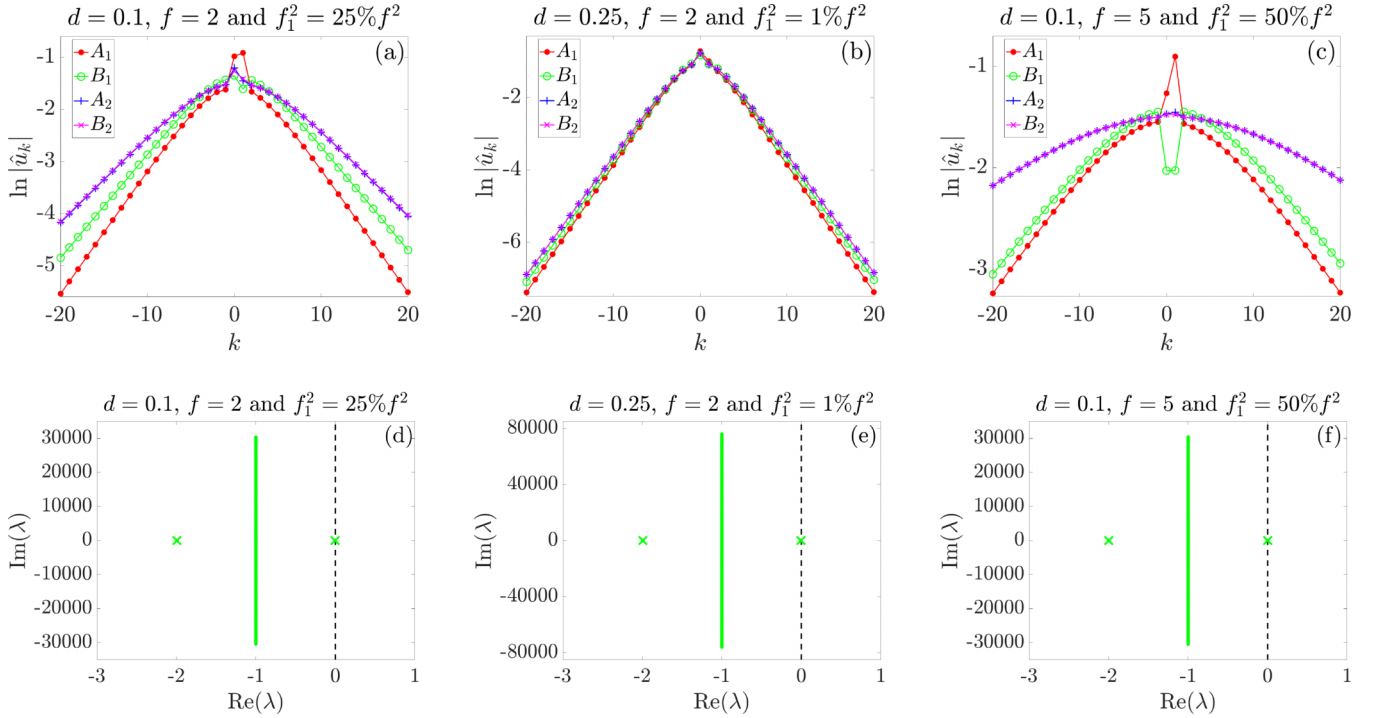


FIG. 1. Every column corresponds to a different choice of d , f , and f_1 . Upper panel [(a)–(c)]: spectral power distributions of the solitons (two ζ_0 steps leading to A_1, A_2 and two ω steps leading to B_1, B_2). Comb lines of A_2, B_2 do not differ significantly. Lower panel [(d)–(f)]: stability plots for B_3 obtained from the third ω step. B_3 is spectrally stable since the eigenvalues of the linearized operator L (green) lie to the left of the imaginary axis (black dashed line). An eigenvalue close to zero occurs since the solitons are found near turning points of the ζ_0 branches.

respect to either the ζ_0 or the ω parameter (while keeping the other parameter fixed) until we detect a soliton u with minimal FWHM of $|u|^2$ in time domain. We stop the algorithm when the relative change of the FWHM between two consecutive solitons is sufficiently small. In our numerical experiments at most three optimizations in both of the variables ζ_0 and ω were sufficient to obtain a relative change in FWHM below 10^{-7} .

In Figs. 1(a)–1(c) we plotted the spectral power distributions of the iterated solitons A_1, B_1, A_2, B_2 for three different choices of the parameters d, f , and f_1 (A_j, B_j are the result of the j th optimization in ζ_0, ω , respectively). It is well visible that the combs get broader after every optimization step. It takes at least one optimization step in ζ_0 and ω so that the solitons position themselves near intensity maxima of the pump. This can be seen also in Fig. 4. The second row of Fig. 1 contains information on the spectral stability of the optimized solitons. This will be explained next.

Stability of optimal solitons. To investigate the stability of the solitons, we use the transformation $a(\tau, x) = b(\tau, x - \omega\tau)$ and decompose $b = b_1 + ib_2$ into real and imaginary parts to rewrite (1) as

$$\begin{aligned} \frac{\partial b_1}{\partial \tau} &= -db_2'' + \omega b_1' - b_1 + \zeta_0 b_2 - (b_1^2 + b_2^2)b_2 \\ &\quad + f_0 + f_1 \cos(k_1 s), \\ \frac{\partial b_2}{\partial \tau} &= db_1' + \omega b_2' - b_2 - \zeta_0 b_1 + (b_1^2 + b_2^2)b_1 + f_1 \sin(k_1 s), \end{aligned} \quad (3)$$

where b is again 2π periodic in s . Solutions u of (2) correspond to stationary solutions $b(\tau, s) = u(s)$ of (3). Spectral stability is based on the following considerations. Let $b(\tau, s) \approx u(s) + [\phi(s) + i\psi(s)]e^{\lambda\tau}$ with 2π -periodic real-valued functions ϕ, ψ , and insert this ansatz into (3). After keeping only the linear terms in ϕ and ψ , we find that ϕ, ψ have to satisfy the eigenvalue equation

$$L \begin{pmatrix} \phi \\ \psi \end{pmatrix} = \lambda \begin{pmatrix} \phi \\ \psi \end{pmatrix},$$

with the linearized operator

$$L = \begin{pmatrix} \omega \frac{d}{ds} - 1 - 2u_1 u_2 & -d \frac{d^2}{ds^2} + \zeta_0 - u_1^2 - 3u_2^2 \\ d \frac{d^2}{ds^2} - \zeta_0 + 3u_1^2 + u_2^2 & \omega \frac{d}{ds} - 1 + 2u_1 u_2 \end{pmatrix}.$$

We see that the perturbation $[\phi(s) + i\psi(s)]e^{\lambda\tau}$ will tend to zero if and only if the eigenvalues λ of L lie in the left complex plane. Using this criterion, we found that the optimized solitons (optimized with respect to ζ_0 and ω by the above algorithm) discussed in this section are all spectrally stable. To show this, we computed the eigenvalues of the finite-element discretization of the operator L and observed that they entirely belong to the left complex plane; cf. Figs. 1(d) and 1(e). One sees that there is always an eigenvalue very close to zero. The reason for this is the following. The solitons with optimal FWHM are found near turning points along branches of the ζ_0 continuation. These turning points are necessarily associated with a zero eigenvalue of the linearized operator L . Hence, for u being in the vicinity of a turning point, there will be an eigenvalue of L very close to zero.

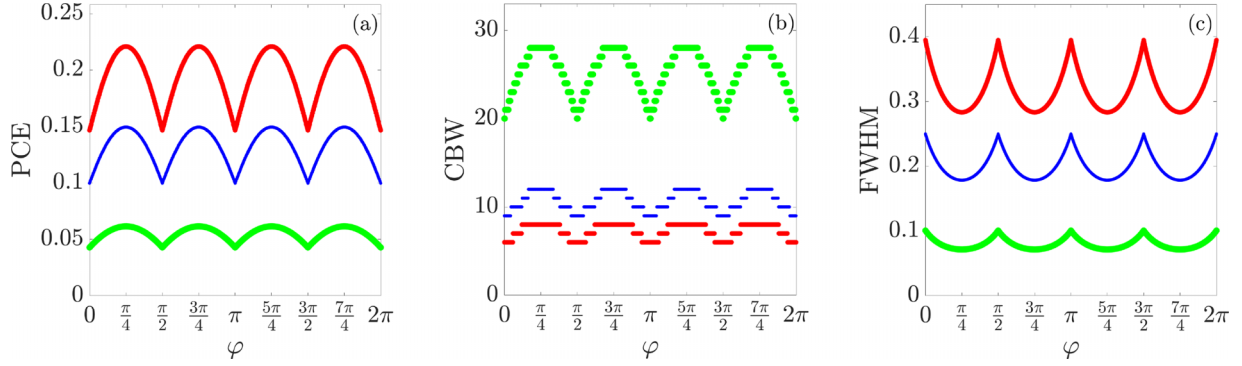


FIG. 2. Power conversion efficiency, comb bandwidth, and full width at half maximum as a function of φ for three different examples. The blue curves correspond to $d = 0.1$ and $f = 2$ and the red ones to $d = 0.25$ and $f = 2$, as well as the green ones to $d = 0.1$ and $f = 5$.

IV. OPTIMAL POWER DISTRIBUTION WHEN PUMPING TWO ADJACENT MODES

In this section we answer the question of which amount of the normalized total input power $f^2 = f_0^2 + f_1^2$ needs to be pumped into each mode in order to obtain the best soliton, i.e., we determine the optimal power distribution between the two pumped modes. The power distribution is described as $(f_0, f_1) = (f \cos \varphi, f \sin \varphi)$ with $\varphi \in [0, 2\pi)$. As before, we assume anomalous dispersion $d > 0$ and fix the indices $k_0 = 0$ and $k_1 = 1$ of the two pumped modes. Additionally, the normalized total input power f^2 is given. Armed with the algorithm from Sec. III we are able to identify for any fixed $\varphi \in [0, 2\pi)$ a 1-soliton with the strongest spatial localization, i.e., with minimal FWHM.

Using this approach, we calculate for each such comb state $u(s) = \sum_{k \in \mathbb{Z}} \hat{u}_k e^{iks}$ the power conversion efficiency (PCE), the comb bandwidth (CBW), and its FWHM. The PCE is defined as the ratio P_{FC}/f^2 between intracavity comb power

$$\begin{aligned} P_{\text{FC}} &= \sum_{k \in \mathbb{Z} \setminus \{0,1\}} |\hat{u}_k|^2 + \frac{f_1^2}{f^2} |\hat{u}_0|^2 + \frac{f_0^2}{f^2} |\hat{u}_1|^2 \\ &= \sum_{k \in \mathbb{Z} \setminus \{0,1\}} |\hat{u}_k|^2 + \sin^2(\varphi) |\hat{u}_0|^2 + \cos^2(\varphi) |\hat{u}_1|^2 \end{aligned}$$

and the normalized total input power. Note that the intracavity comb power is a weighted sum over the power in each mode. The weights f_j^2/f^2 , $j = 0, 1$ of the power of the zero mode and the first mode are such that $f_1 = 0$ or $f_0 = 0$ lead to the usual definition of PCE and $f_0 \rightarrow \infty$ or $f_1 \rightarrow \infty$ lead to an exclusion of the power contributed by the zero or first mode, respectively. The CBW is defined via the 3 dB points, i.e.,

$$\text{CBW} = k_l^* + k_r^*,$$

with minimal integers $k_l^* > 0$ and $k_r^* > 0$ which fulfill

$$|\hat{u}_{-k_l^*}|^2 \leq \frac{1}{2} |\hat{u}_{-1}|^2, \quad |\hat{u}_{1+k_r^*}|^2 \leq \frac{1}{2} |\hat{u}_2|^2,$$

respectively. Note that the 3 dB comb bandwidth is defined with respect to the power $|\hat{u}_{-1}|^2$ and $|\hat{u}_2|^2$ of the modes directly adjacent to the pumped modes rather than the power $|\hat{u}_0|^2$ and $|\hat{u}_1|^2$ of the pumped modes themselves.

To find the optimal power distribution between the zero mode and the first mode we performed a parameter study in

φ for three different examples; cf. Fig. 2. In the first example we chose $d = 0.1$ and $f = 2$ and in the second example we kept $f = 2$ but changed the dispersion to $d = 0.25$, while in the last example we kept $d = 0.1$ and changed the forcing to $f = 5$. For these three examples we computed the most localized 1-soliton for $\varphi \in [0, 2\pi)$ based on the algorithm of Sec. III and evaluated the PCE and the CBW as well as the FWHM of the resulting comb state.

The results depicted in Fig. 2 clearly demonstrate the advantages of dual-tone pumping, in particular when using equal power in both modes. In all of the examples PCE and CBW increase while the FWHM decreases with $\varphi \in [0, \pi/4]$. Moreover, as we will explain at the end of this section, PCE, CBW, and FWHM are $\pi/2$ periodic and symmetric with respect to $\pi/4$. We conclude that (i) pumping two modes is advantageous to pumping only one mode, (ii) PCE, CBW, and FWHM are monotonic functions of $|f_0| + |f_1| = |f|(|\cos \varphi| + |\sin \varphi|)$, and (iii) the optimal case arises for equal pump powers $|f_0| = |f_1|$.

In Figs. 3(a) and 3(b) we plotted the optimal values of ζ_0 and ω (for which the most localized soliton was found) against φ . Since $k_1 = 1$ we have $\omega = \Delta\zeta + d$ so that the optimal value of ω can be easily translated into an optimal value of $\Delta\zeta$. We added in Fig. 3(c) a plot of the optimal value of $\Delta\zeta$ against φ since the normalized detuning difference $\Delta\zeta = \zeta_0 - \zeta_1$ is the physically more tangible quantity, while from a mathematical point of view it is more convenient to work with ω . In all of the examples the optimal values of ζ_0 , ω , and $\Delta\zeta$ increase with $\varphi \in (0, \pi/4]$. Once again we observe several symmetries, which we will address in the end of this section. We further conclude that (iv) the optimal value of ζ_0 is almost independent of d , (v) the optimal value of ω is almost independent of f , and (vi) the optimal value of ω coincides with the dispersion d in the case of optimal power distribution $|f_0| = |f_1|$.

As $\omega = \Delta\zeta + d$, (vi) means $\Delta\zeta = 0$, i.e., optimal solitons require equal detuning distances $\omega_0 - \omega_{p_0} = \omega_1 - \omega_{p_1}$ in the case of equal power distribution $|f_0| = |f_1|$. From Fig. 3(c) we further find that the optimal values for ζ_0 and ζ_1 satisfy the relation $|f_0| > |f_1| \Leftrightarrow \zeta_0 < \zeta_1$, i.e., pumping more power into one mode is compensated by a larger detuning for the second mode.

For each of the three examples from Figs. 2 and 3 we added in Fig. 4 plots of the spatial and spectral power distributions

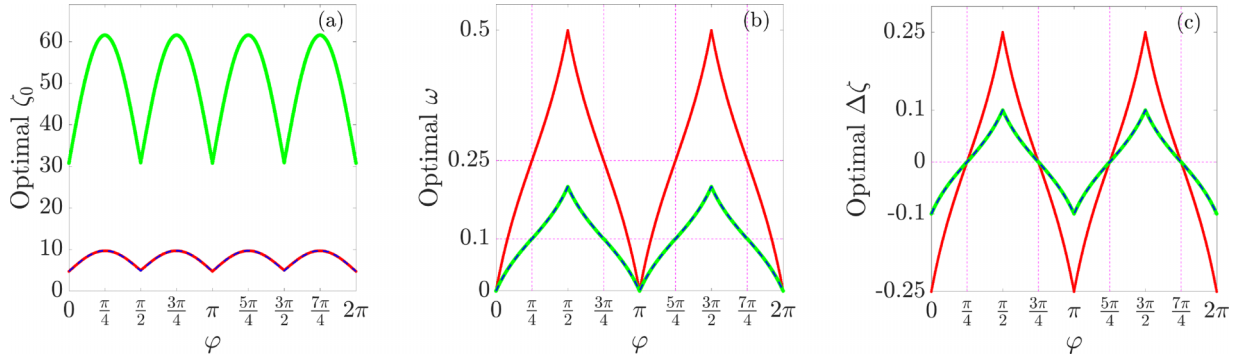


FIG. 3. Optimal values of ζ_0 , ω , and $\Delta\zeta$ as a function of φ for three different examples. The blue curves correspond to $d = 0.1$ and $f = 2$ and the red ones to $d = 0.25$ and $f = 2$, as well as the green ones to $d = 0.1$ and $f = 5$. The blue and the red curves in (a) as well as the blue and the green curves in (b) and (c) are plotted dashed so that one of the curves is not completely covered by the other one. The dashed lines colored in magenta in (b) emphasize that the optimal value of ω coincides with the dispersion d in the optimal case $|f_0| = |f_1|$, where $\varphi \in \{\pi/4, 3\pi/4, 5\pi/4, 7\pi/4\}$. The dashed lines colored in magenta in (c) emphasize that the optimal value of $\Delta\zeta$ vanishes in the optimal case $|f_0| = |f_1|$, where $\varphi \in \{\pi/4, 3\pi/4, 5\pi/4, 7\pi/4\}$.

of the optimal solitons for selected values of $\varphi \in [0, \pi/4]$. In this range for φ we have $f_0, f_1 \geq 0$. The particular values of φ are chosen as $f_0^2 = 100\%f^2$ (one mode case), $f_0^2 = 90\%f^2$ (slight perturbation of the one mode case), and $f_0^2 = 50\%f^2$ (optimal two mode case). We have chosen a logarithmic scale for the spatial power distribution to highlight the nonconstant background of the solitons. Since for $f_1 > 0$ there is no shift invariance in (2) anymore all of the depicted solitons are localized around $s = 0$, which is the unique point in the interval $[0, 2\pi)$, where the absolute value of the pump power is maximal, i.e., $f^2 + 2f_0f_1 = \max_{s \in [0, 2\pi)} |if_0 + if_1e^{is}|^2$. In

other words, the best soliton positions its maximum at the point where the pump has maximal power and its background follows qualitatively the shape of the pump.

In the time domain, with only one pumped mode, the pump power is constant and so is the background. In contrast, with a second pumped mode, the pump profile becomes sinusoidal with a peak at $s = 0$, and in particular the peak pump power is higher than the pump power in the one mode case (provided we keep the same total input power). Physically, only the fraction of the pump that overlaps temporally with the soliton pulse can effectively power the soliton. We observe that the

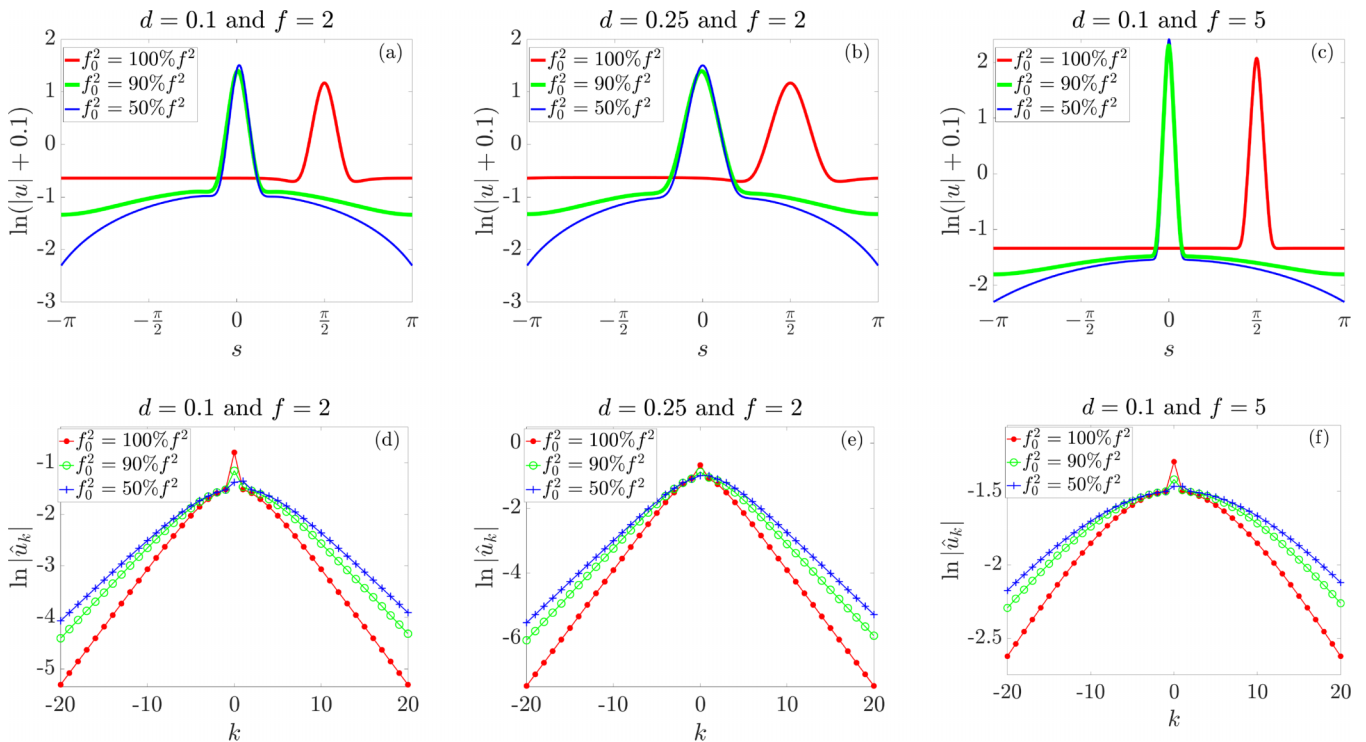


FIG. 4. Spatial and spectral power distributions of optimal solitons for selected values of $\varphi \in [0, \pi/4]$, which correspond to $f_0^2 = 100\%f^2$ and $f_0^2 = 90\%f^2$, as well as $f_0^2 = 50\%f^2$ for three different examples. Every column corresponds to one example. The logarithmic scale in [(a)–(c)] was chosen to highlight the nonconstant background of the solitons.

generated optimized soliton makes use of the sinusoidal peak pump power profile and positions itself at $s = 0$ where the pump power is maximal, which leads to an improved pump to soliton-pulse power conversion efficiency [30,31]. As expected, the peak power of the soliton is then also improved compared to the one mode case. But apparently, this is not the case for the background and the quantitative relation between soliton background and pump shape is more subtle. Finally, for fixed total input power $f^2 = f_0^2 + f_1^2$, the peak power of the pump $f^2 + 2f_0f_1$ is maximal for $f_0 = f_1 = f/\sqrt{2}$, i.e., it is attained when the power distribution between the two pumped modes is equal. This leads to the optimal pump to soliton power conversion efficiency. Let us point out that our findings on the position of the optimized solitons are in contrast to [30,32]. In [30] the authors explain that the solitons position themselves off the peak of the driving field and how this is influenced by detuning of the pumping rate, the normalized pump-cavity detuning, the pumping field profile, and additionally by taking the Raman effect into consideration. In [32] a similar effect is described in dependency on the driving field peak amplitude and pump-cavity detuning. The major difference is that in our case the detuning variables ζ_0, ζ_1 and thus ζ_0, ω as well as the distribution of input power between the two modes are completely free and subject to the optimization, whereas in [30,32] optimization with respect to these degrees of freedom was not part of the investigation.

Finally, we explain the symmetry properties of Figs. 2 and 3 from the symmetries of (2). If u solves (2) then $u(\cdot + \pi)$ solves (2) with f_1 replaced by $-f_1$ and $-u(\cdot + \pi)$ solves (2) with f_0 replaced by $-f_0$. This means that the signs of f_0 and f_1 are not relevant for the curves in Figs. 2 and 3. The symmetry with respect to $\pi/4$ of the curves in Fig. 2 stems from the interchangeability of f_0 and f_1 . Namely, if u solves (2) with given values of ζ_0, ω then $v(s) := u(-s)e^{is}$ solves

$$-dv'' + i\tilde{\omega}v' - (i - \zeta_1)v - |v|^2v + if_1 + if_0e^{is} = 0,$$

with $\zeta_1 = \zeta_0 - \omega + d$ and $\tilde{\omega} = 2d - \omega$. Note that the roles of f_0 and f_1 are now interchanged. The fact that ζ_0 and ω have changed to ζ_1 and $\tilde{\omega}$ is not relevant since we optimize anyway in these parameters. Together with (vi) this also explains that the curves in Figs. 3(b) and 3(c) are odd with respect to the points $(\pi/4, d)$ and $(\pi/4, 0)$, respectively. We also mention that the curves in Fig. 3(a) are not symmetric with respect

to $\pi/4$ but this is not visible in the plot since the difference $\Delta\zeta = \zeta_0 - \zeta_1 = \omega - d$ is small compared to ζ_0 and ζ_1 .

V. TRENDS FOR VARYING FORCING AND VARYING DISPERSION

For the results in this section we have carried out a parameter study with respect to dispersion d and normalized pump amplitude f , considering the behavior of PCE, CBW, and FWHM of the best solitons (i.e., minimal FWHM) under optimal power distribution $f_0 = f_1 = f/\sqrt{2}$. As before, we have fixed the two pumped modes to $k_0 = 0$ and $k_1 = 1$. We have considered dispersion parameters $d = 0.1, 0.15, 0.2, 0.25$ and normalized total pump amplitude $f \in (0, 10]$. From Sec. IV we know that under optimal power distribution the solitons with minimal FWHM arise for $\omega = d$. Using this information we can reduce the algorithm of Sec. III to a single optimization step in ζ_0 . Since $f_0 = f_1$ we see that now PCE is the ratio between

$$P_{\text{FC}} = \sum_{k \in \mathbb{Z} \setminus \{0,1\}} |\hat{u}_k|^2 + \frac{1}{2}|\hat{u}_0|^2 + \frac{1}{2}|\hat{u}_1|^2$$

and the total pump power f^2 .

The results are shown in Fig. 5. We observe the following trends: CBW increases, whereas FWHM and PCE decrease with increasing forcing f . Additionally, one can see that with $d \rightarrow 0^+$ once again CBW increases and FWHM and PCE decrease. These observations are in good agreement with the trends from the one mode case; cf. [20]. Further, one can observe in Fig. 5(c) that FWHM tends to π as $f \rightarrow 0^+$. This can be understood as follows: as $f \rightarrow 0^+$ the solutions of (2) tend to zero and behave like the solutions of the linear equation

$$-du'' + i\omega u' - (i - \zeta_{0,\text{opt}})u + if_0 + if_1e^{is} = 0.$$

Since $d = \omega$ for optimal solitons under optimal power distribution $f_0 = f_1 = f/\sqrt{2}$ the above linear equation is solved by

$$u(s) = \frac{if}{\sqrt{2}(i - \zeta_{0,\text{opt}})}(1 + e^{is})$$

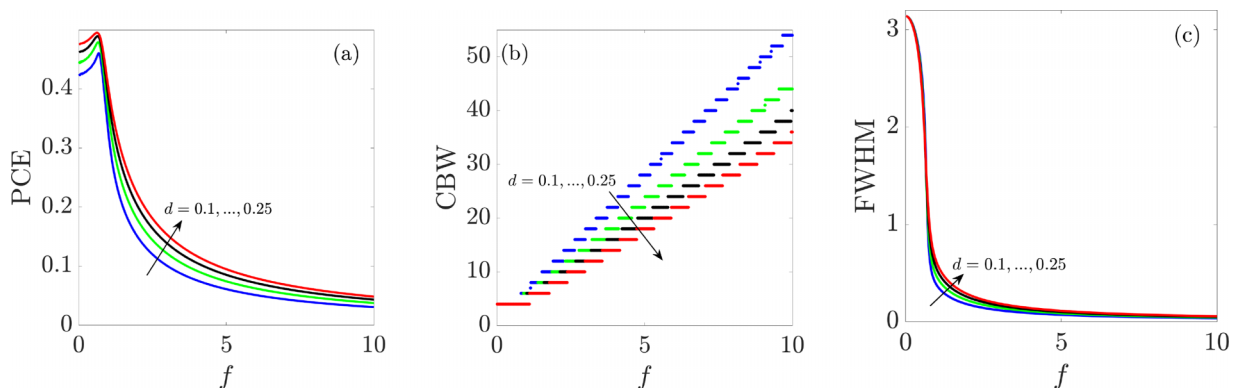


FIG. 5. Power conversion efficiency, comb bandwidth, and full width at half maximum as a function of the forcing f and dispersion $d = 0.1, 0.15, 0.2, 0.25$.

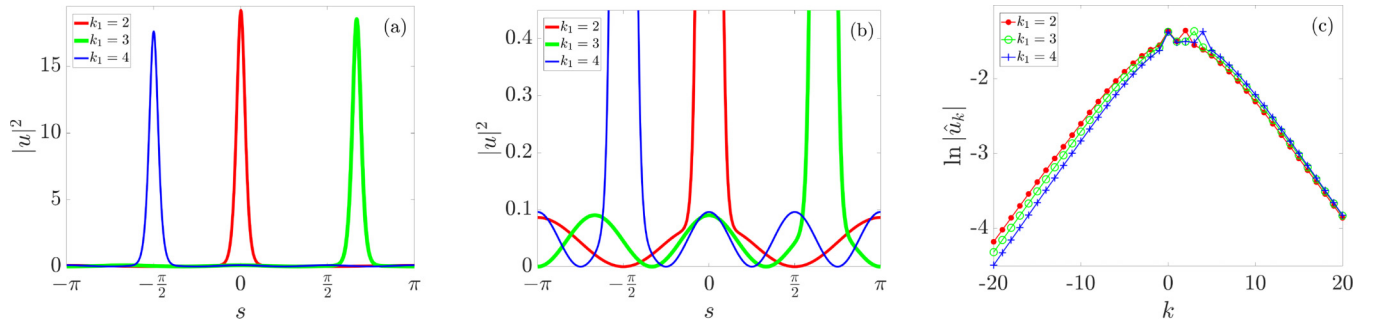


FIG. 6. Spatial and spectral power distributions of the optimal 1-solitons from the case $d = 0.1$ and $f_0 = f_1 = \sqrt{2}$ for $k_1 = 2, 3, 4$. Plot (b) is a zoom of plot (a), which highlights the background of the solitons.

and the latter has a FWHM of π . Similarly, in agreement with Fig. 5(a), we have

$$\text{PCE}(u) \rightarrow \frac{1}{2(1 + \zeta_{0,*}^2)} \leq \frac{1}{2}$$

as $f \rightarrow 0^+$, where we assume $\zeta_{0,*} = \lim_{f \rightarrow 0^+} \zeta_{0,\text{opt}}$.

Finally we mention that the jumps of size two in Fig. 5(b) could be caused by our choice of the discretization of the f interval $(0,10]$. It is possible that a finer discretization would lead to more plausible jumps of size one. Nevertheless, the finer discretization, which leads to significantly longer run times of the code, has no essential effect on the trends of the curves.

VI. 1-SOLITONS OBTAINED FROM PUMPING TWO ARBITRARILY DISTANCED MODES IN A PURELY SECOND-ORDER DISPERSION CASE

For large distances between the two pumped modes, we would need to take into account higher-order dispersion. Higher-order dispersion effects together with pumping modes from different mode families were considered in [33]. In the following considerations, however, we restrict to second-order dispersion and to modes coming from the same mode family. In the case where the pumped modes are $k_0 = 0$ and $k_1 \geq 2$ we have a heuristic algorithm which enables us to identify a 1-soliton with the strongest spatial localization. The algorithm is based on a variant of the one from the case $k_1 = 1$, cf. Sec. III, and details can be found in Appendix B. Applying this algorithm our experiments suggest that the optimal power distribution is again given by the equal distribution $|f_0| = |f_1|$ as in the case $k_1 = 1$. Moreover, for equal power distribution, $\omega = k_1 d$ turns out to be optimal, which once again translates into equal detuning offsets $\Delta\zeta = 0$. In Fig. 6(a) we plotted the spatial power distributions of the optimal 1-solitons from the case $d = 0.1$ and $f_0 = f_1 = \sqrt{2}$ for $k_1 = 2, 3, 4$. One can observe that the optimal 1-soliton gets less localized as k_1 increases. In Fig. 6(b) we added a zoom in to better point out the background of the solitons. Since with u also $u(\cdot + 2\pi/k_1)$ is a solution of (2) optimal 1-solitons can be shifted by multiples of $2\pi/k_1$. We see that the 1-soliton localizes once again around one of the points where the absolute value of the pump term $if_0 + if_1 e^{ik_1 s}$ is maximized. In Fig. 6(c) we added the spectral power distributions of the optimal 1-solitons. Nec-

essarily each comb is peaked at the pumped modes $k_0 = 0$ and k_1 .

VII. SUMMARY

We have considered pumping two different modes for a Kerr nonlinear microresonator with anomalous dispersion. Using numerical path continuation and optimization methods we found and tested an algorithm which allows one to find for fixed normalized total pump power the optimal detuning offsets that provide the most localized 1-soliton. The algorithm applies in its simple form to the case of pumping two adjacent modes and in a more refined form (taking bifurcations into account) also to the case of pumping two arbitrarily distanced modes. Optimal 1-solitons appear to be spectrally stable and localize themselves around the intensity maxima of the pump. While it became clear that pumping two modes is always advantageous to pumping one mode, in the case of pumping two adjacent modes we went deeper into the question of how the normalized total input power should be divided into the two pumped modes in order to optimize quality metrics like PCE, CBW, and FWHM. A detailed parameter study shows that the optimal distribution is always the equal distribution $|f_0| = |f_1| = |f|/\sqrt{2}$ with equal detuning offsets. The situation appears to be similar in the case of pumping two arbitrarily distanced modes. Our approach has thus validated the assumptions in [10]. Finally, we determined trends of PCE, CBW, and FWHM by varying anomalous dispersion and normalized total input power. The trends are in good agreement with the case of pumping only one mode; cf. [20]. Our approach is well suited to determining and analyzing optimal pumping schemes in the case where more than two modes are pumped.

ACKNOWLEDGMENT

Funded by the Deutsche Forschungsgemeinschaft (DFG, German Research Foundation), Project-ID 258734477-SFB 1173.

APPENDIX A: DERIVATION OF THE LUGIATO-LEFEVER MODEL FOR A DUAL-PUMPED RING RESONATOR

In this section we derive (1) from a system of coupled-mode equations; cf. [16,34]. When a resonant cavity is

pumped by two continuous wave lasers with frequencies ω_{p_0} and ω_{p_1} a system of nonlinear coupled-mode equations can be used to describe the evolution of the field inside the cavity. The numbering k of the resonant modes in the cavity is relative to the mode $k_0 = 0$. We use the cold cavity dispersion relation $\omega_k = \omega_0 + d_1 k + d_2 k^2$ for the resonant frequencies ω_k , where d_1 corresponds to the FSR of the resonator and $2d_2$ to the difference between two neighboring FSRs at the center frequency ω_0 . With $\tilde{k}_0, \tilde{k}_1 \in \mathbb{Z}$, $\tilde{k}_0 < \tilde{k}_1$, we denote the two pumped modes. If \hat{A}_k is the mode amplitude of the k th resonant mode normalized such that $|\hat{A}_k|^2$ is the number of quanta in the k th mode, then the simplified set of equations reads as follows; cf. [16,34]:

$$\begin{aligned} \frac{\partial \hat{A}_k}{\partial t} = & -\frac{\kappa}{2} \hat{A}_k + \sum_{j=0}^1 \delta_{\tilde{k}\tilde{k}_j} \sqrt{\kappa_{\text{ext}} s_j} e^{-i(\omega_{p_j} - \omega_{\tilde{k}_j})t} e^{i\phi_j} \\ & + ig \sum_{k'+k''-k'''=k} \hat{A}_{k'} \hat{A}_{k''} \hat{A}_{k'''} e^{-i(\omega_{k'} + \omega_{k''} - \omega_{k'''} - \omega_k)t}. \end{aligned} \quad (\text{A1})$$

Here, $\kappa = \kappa_0 + \kappa_{\text{ext}}$ denotes the cavity decay rate as a sum of intrinsic decay rate κ_0 and coupling rate to the waveguide κ_{ext} and ϕ_0, ϕ_1 are the initial phases of the pumps. If $P_{\text{in},0}, P_{\text{in},1}$ are the powers of the two input lasers, then $s_j = \sqrt{P_{\text{in},j}/\hbar\omega_{\tilde{k}_j}}$, $j = 0, 1$ are the powers coupled to the cavity. The nonlinear coupling coefficient

$$g = \frac{\hbar\omega_0^2 c n_2}{n_0^2 V_{\text{eff}}}$$

denotes a per photon frequency shift of the cavity due to the Kerr nonlinearity and thus describes the strength of the cubic nonlinearity of the system with linear refractive index n_0 , nonlinear refractive index n_2 , and effective cavity nonlinear volume V_{eff} . Finally, c is the vacuum speed of light and \hbar is the Planck constant.

By using the transformation

$$\tilde{a}(\tau, x) := \sqrt{\frac{2g}{\kappa}} \sum_{k \in \mathbb{Z}} \hat{A}_k \left(\frac{2}{\kappa} \tau \right) e^{-idk^2\tau} e^{ikx},$$

the system (A1) of coupled-mode equations may be rewritten in a dimensionless way as a partial differential equation,

$$\begin{aligned} i \frac{\partial \tilde{a}}{\partial \tau} = & -d\tilde{a}'' - i\tilde{a} - |\tilde{a}|^2 \tilde{a} + i \sum_{j=0}^1 f_j e^{i(\tilde{k}_j x - \tilde{\nu}_j \tau + \phi_j)}, \\ & \tilde{a} \text{ } 2\pi \text{ periodic in } x, \end{aligned} \quad (\text{A2})$$

where $\tau = \kappa t/2$, $d = 2d_2/\kappa$, and $\zeta_j = 2(\omega_{\tilde{k}_j} - \omega_{p_j})/\kappa$, $\tilde{\nu}_j = d\tilde{k}_j^2 - \zeta_j$, $\eta = \kappa_{\text{ext}}/\kappa$, $f_j = \sqrt{8\eta g/\kappa^2 s_j}$ for $j = 0, 1$. By setting

$$a(\tau, x) := e^{-i(\tilde{k}_0(x+2d\tilde{k}_0\tau - \psi) - \tilde{\nu}_0\tau + \phi_0)} \tilde{a}(\tau, x + 2d\tilde{k}_0\tau - \psi),$$

with $\psi = (\phi_1 - \phi_0)/k_1$, we find that a satisfies (1) with $k_1 = \tilde{k}_1 - \tilde{k}_0$, $\Delta\zeta = \zeta_0 - \zeta_1$, and $\nu_1 = \tilde{\nu}_1 - \tilde{\nu}_0 - 2dk_0k_1 = \Delta\zeta + dk_1^2$. Thus we can always assume, for simplicity, that the pumped modes are $k_0 = 0$ and $k_1 \in \mathbb{N}$ and that the initial phase of both pumps is zero. Moreover, we see that the change from \tilde{a} to a shifts the time-dependent Fourier coefficients from \hat{A}_k to $\hat{A}_{k+\tilde{k}_0}$ and multiplies them with $e^{-i(\zeta_0\tau + \phi_0 + k\psi)}$ so that

the power in each individual mode is (up to an index shift) preserved.

Finally, let us explain that the intracavity power $P = \sum_{k \in \mathbb{Z}} |\hat{u}_k|^2 = \frac{1}{2\pi} \int_0^{2\pi} |u(s)|^2 ds$ of a 2π -periodic traveling-wave comb state u cannot exceed the normalized total input power $f^2 = f_0^2 + f_1^2$. To see this, we multiply the equation (2) for the traveling-wave profile u with $\bar{u}(s)$ and take the imaginary part to obtain

$$\begin{aligned} -d \text{Im}[u''(s)\bar{u}(s)] + \omega \text{Re}[u'(s)\bar{u}(s)] - |u(s)|^2 \\ + \text{Re}[(f_0 + f_1 e^{ik_1 s})\bar{u}(s)] = 0. \end{aligned}$$

Integration over the interval $[0, 2\pi]$, using integration by parts for the first term and $\frac{d}{ds}|u(s)|^2 = 2 \text{Re}[u'(s)\bar{u}(s)]$ for the second term together with the Cauchy-Schwarz inequality, yields

$$\begin{aligned} \int_0^{2\pi} |u(s)|^2 ds = \int_0^{2\pi} \text{Re}[(f_0 + f_1 e^{ik_1 s})\bar{u}(s)] ds \\ \leq \left(\int_0^{2\pi} |u(s)|^2 ds \right)^{1/2} \sqrt{2\pi} (f_0^2 + f_1^2)^{1/2} \end{aligned}$$

and hence $\frac{1}{2\pi} \int_0^{2\pi} |u(s)|^2 ds \leq f_0^2 + f_1^2$.

APPENDIX B: FINDING LOCALIZED SOLITONS IN THE CASE OF PUMPING TWO ARBITRARILY DISTANCED MODES

By considering additional bifurcations we will demonstrate how the optimization algorithm from Sec. III can be adapted to arbitrary values of $k_1 \geq 2$. A first observation is that the very same algorithm as used in Sec. III would lead to solitons which are not only 2π but in fact $2\pi/k_1$ periodic, i.e., the algorithm detects no 1-solitons. This is essentially due to the fact that starting from a constant solution any kind of parameter continuation will develop solutions that have the shape of the pump.

However, in contrast to the case $k_1 = 1$, we also detect bifurcations this time. The idea of the adapted algorithm is to switch in every ζ_0 -optimization step to a bifurcating branch containing 1-solitons. For $d = 0.1$, $f = 2$, and $f_1^2 = 25\% f^2$, this is illustrated in Figs. 7(a) and 7(d) for $k_1 = 2, 3$. The gray branch is the new additional branch bifurcating from the first continued (blue) branch in ζ_0 and A_1 indicates the optimal point with the minimal FWHM on that branch. The point A_1 is then used as the starting point for the subsequent ω optimization and from here on we can once again iterate the whole process.

The mentioned bifurcations turn out to be not of a simple nature in general. For example, if k_1 is odd, `path` detects no bifurcations at all (which may be due to an even number of eigenvalues crossing zero simultaneously). However, we can easily overcome this issue by using an interpolation trick for branch switching. For that, we consider a ζ_0 value near a turning point, where we find two distinct solutions (named X and Y) for one and the same value of ζ_0 . In Fig. 7(a) we used $\zeta_0 = 3.3$ and in Fig. 7(d) we used $\zeta_0 = 3.1$ for this purpose and marked the mentioned solutions in red and green, respectively. Figures 7(b) and 7(e) show the spatial power distributions of X and Y . It turns out that a 1-soliton-like

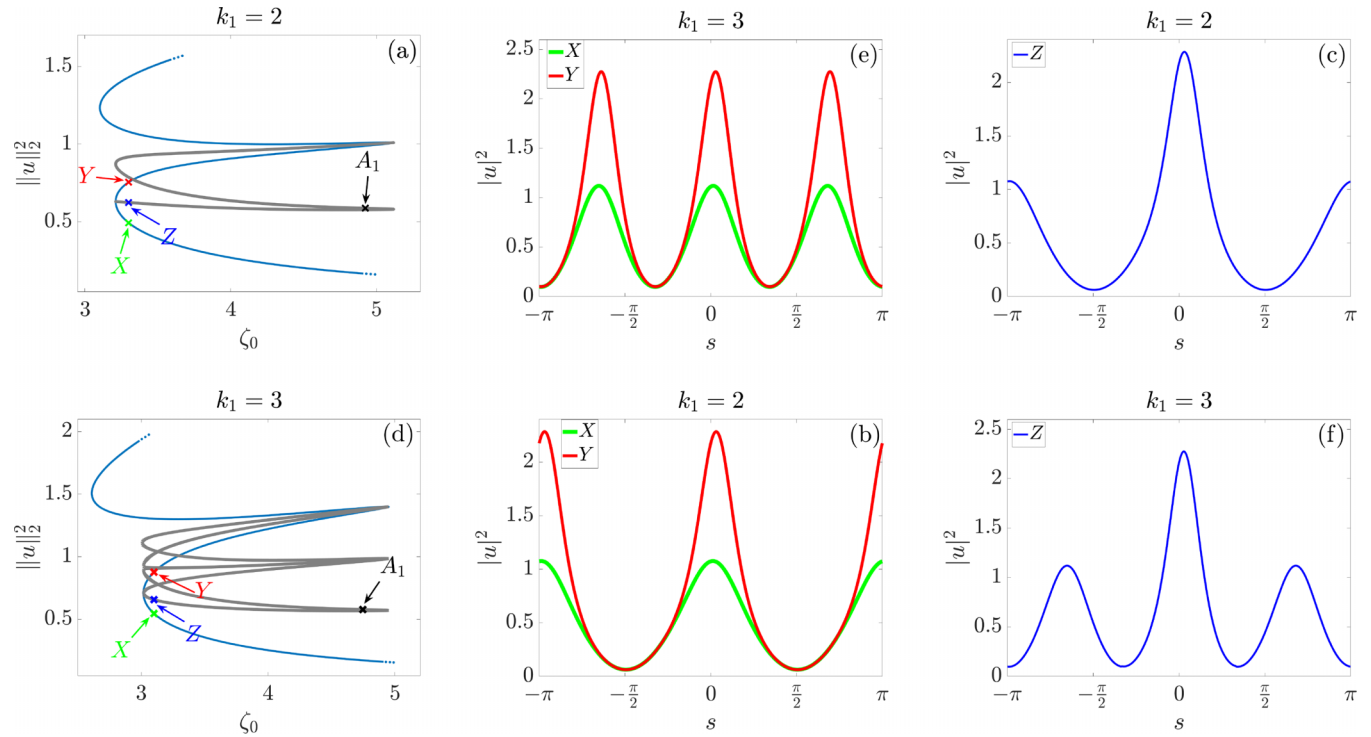


FIG. 7. Example for $d = 0.1$, $f = 2$, and $f_1^2 = 25\%f^2$. First column: branches show intracavity power $\|u\|_2^2 = \frac{1}{2\pi} \int_0^{2\pi} |u(s)|^2 ds$ of the soliton u plotted vs ζ_0 . Blue branch as achieved by first ζ_0 optimization and gray branch obtained from first bifurcation from blue branch. A_1 indicates the optimal point with minimal FWHM. Second and third column: spatial power distribution of solutions used for branch switching. Plots [(a)–(c)] correspond to the case $k_1 = 2$, while plots [(d)–(f)] correspond to $k_1 = 3$.

state, which is not $2\pi/k_1$ periodic anymore, can be glued together from parts of these solutions. The resulting soliton Z is marked in blue in Figs. 7(a) and 7(d) and its spatial power distribution is given in Figs. 7(c) and 7(f). The interpolated

soliton serves as the starting point for another ζ_0 optimization yielding the gray branch, which actually is a branch which bifurcates from the original curve and connects two of its turning points.

-
- [1] T. Udem, R. Holzwarth, and T. W. Hänsch, *Nature (London)* **416**, 233 (2002).
- [2] N. Picqué and T. W. Hänsch, *Nat. Photon.* **13**, 146 (2019).
- [3] Q.-F. Yang, M.-G. Suh, K. Y. Yang, X. Yi, and K. J. Vahala, *CLEO: Science and Innovations* (Optica Publishing Group, Washington, DC, 2017), pp. SM4D–4.
- [4] D. J. Jones, S. A. Diddams, J. K. Ranka, A. Stentz, R. S. Windeler, J. L. Hall, and S. T. Cundiff, *Science* **288**, 635 (2000).
- [5] D. T. Spencer, T. Drake, T. C. Briles, J. Stone, L. C. Sinclair, C. Fredrick, Q. Li, D. Westly, B. R. Ilic, A. Bluestone *et al.*, *Nature (London)* **557**, 81 (2018).
- [6] Z. L. Newman, V. Maurice, T. Drake, J. R. Stone, T. C. Briles, D. T. Spencer, C. Fredrick, Q. Li, D. Westly, B. R. Ilic *et al.*, *Optica* **6**, 680 (2019).
- [7] P. Trocha, M. Karpov, D. Ganin, M. H. Pfeiffer, A. Kordts, S. Wolf, J. Krockenberger, P. Marin-Palomo, C. Weimann, S. Randel *et al.*, *Science* **359**, 887 (2018).
- [8] P. Marin-Palomo, J. N. Kemal, M. Karpov, A. Kordts, J. Pfeiffer, M. H. Pfeiffer, P. Trocha, S. Wolf, V. Brasch, M. H. Anderson *et al.*, *Nature (London)* **546**, 274 (2017).
- [9] T. J. Kippenberg, R. Holzwarth, and S. A. Diddams, *Science* **332**, 555 (2011).
- [10] T. Hansson and S. Wabnitz, *Phys. Rev. A* **90**, 013811 (2014).
- [11] V. E. Lobanov, G. Lihachev, and M. L. Gorodetsky, *EPL (Europhys. Lett.)* **112**, 54008 (2015).
- [12] S. B. Papp, P. Del’Haye, and S. A. Diddams, *Opt. Express* **21**, 17615 (2013).
- [13] D. V. Strekalov and N. Yu, *Phys. Rev. A* **79**, 041805(R) (2009).
- [14] S. Zhang, J. M. Silver, L. D. Bino, F. Copie, M. T. M. Woodley, G. N. Ghalanos, A. Ó. Svela, N. Moroney, and P. Del’Haye, *Optica* **6**, 206 (2019).
- [15] W. Weng, R. Bouchand, and T. J. Kippenberg, *Phys. Rev. X* **10**, 021017 (2020).
- [16] H. Taheri, A. B. Matsko, and L. Maleki, *Eur. Phys. J. D* **71**, 153 (2017).
- [17] L. A. Lugiato and R. Lefever, *Phys. Rev. Lett.* **58**, 2209 (1987).
- [18] C. Godey, I. V. Balakireva, A. Coillet, and Y. K. Chembo, *Phys. Rev. A* **89**, 063814 (2014).

- [19] P. Parra-Rivas, D. Gomila, L. Gelens, and E. Knobloch, *Phys. Rev. E* **97**, 042204 (2018).
- [20] J. Gärtner, P. Trocha, R. Mandel, C. Koos, T. Jahnke, and W. Reichel, *Phys. Rev. A* **100**, 033819 (2019).
- [21] C. Godey, *Eur. Phys. J. D* **71**, 131 (2017).
- [22] P. Parra-Rivas, D. Gomila, F. Leo, S. Coen, and L. Gelens, *Opt. Lett.* **39**, 2971 (2014).
- [23] P. Parra-Rivas, E. Knobloch, D. Gomila, and L. Gelens, *Phys. Rev. A* **93**, 063839 (2016).
- [24] R. Mandel and W. Reichel, *SIAM J. Appl. Math.* **77**, 315 (2017).
- [25] T. Miyaji, I. Ohnishi, and Y. Tsutsumi, *Physica D* **239**, 2066 (2010).
- [26] L. Delcey and M. Haragus, *Philos. Trans. R. Soc. A* **376**, 20170188 (2018).
- [27] N. Périnet, N. Verschueren, and S. Coulibaly, *Eur. Phys. J. D* **71**, 243 (2017).
- [28] H. Uecker, D. Wetzel, and J. D. Rademacher, *NMTMA* **7**, 58 (2019).
- [29] T. Dohnal, J. Rademacher, H. Uecker, and D. Wetzel, [arXiv:1409.3119](https://arxiv.org/abs/1409.3119).
- [30] J. Li, C. Bao, Q.-X. Ji, H. Wang, L. Wu, S. Leifer, C. Beichman, and K. Vahala, *Optica* **9**, 231 (2022).
- [31] E. Obrzud, S. Lecomte, and T. Herr, *Nat. Photon.* **11**, 600 (2017).
- [32] I. Hendry, W. Chen, Y. Wang, B. Garbin, J. Javaloyes, G.-L. Oppo, S. Coen, S. G. Murdoch, and M. Erkintalo, *Phys. Rev. A* **97**, 053834 (2018).
- [33] S. Zhang, J. M. Silver, T. Bi, and P. Del’Haye, *Nat. Commun.* **11**, 6384 (2020).
- [34] T. Herr, K. Hartinger, J. Riemensberger, C. Y. Wang, E. Gavartin, R. Holzwarth, M. L. Gorodetsky, and T. J. Kippenberg, *Conference on Lasers and Electro-Optics 2012* (Optica Publishing Group, Washington, DC, 2012), p. QF3G.7.